Two-Pronged Jet Formation Caused by Droplet Impact on Anisotropic Superhydrophobic Surfaces

J. T. Pearson
Department of Mechanical Engineering,
Brigham Young University,
Provo, UT 84602

D. Bilodeau
Department of Mechanical Engineering,
Brigham Young University,
Provo, UT 84602

D. Maynes[1]
Department of Mechanical Engineering,
Brigham Young University,
Provo, UT 84602
e-mail: maynes@byu.edu

When a liquid droplet impacts a superhydrophobic surface with anisotropic surface patterning in the form of alternating ribs and cavities, the rebounding droplet may exhibit a unique two-pronged jet emission. Droplet impact experiments with 11 different fluids of viscosity that varied by more than three orders of magnitude were conducted, and this paper quantifies the Capillary number, Ca, and Ohnesorge number, Oh, ranges over which the two-pronged phenomenon occurs. For $Oh > 0.0154$, the behavior was never observed, while at lower values of Oh, the behavior occurs for an intermediate range of Ca that depends on Oh.
[DOI: 10.1115/1.4032596]

Keywords: superhydrophobic, jet, droplet, impact, two-pronged

1 Introduction

Droplet impact on surfaces has received considerable attention in the past [1], with renewed interest recently motivated by advances in the fabrication of superhydrophobic surfaces [2,3]. When a liquid droplet impinges on a hydrophobic surface at sufficiently high impact speed, it flattens and spreads radially outward in a radially expanding film flow, with the thin film region being surrounded by a capillary rim. Surface tension forces pull inward on the expanding droplet and eventually a maximum spread diameter is reached and the droplet then collapses inward on itself. The maximum spread diameter has received particular emphasis in the literature for a variety of surfaces [4–6], with Marengo et al. providing a review of droplet impact on flat and structured surfaces [7].

Superhydrophobic surfaces are fabricated with the combination of microscale surface patterning and a thin-film hydrophobic coating. Provided the Cassie state is maintained [8], liquid will wet only the top of the microscale patterned features on the surface over most of the spreading thin film region, although at the impact point wetting of the patterned surface generally always occurs [9]. Consequently, an apparent slip velocity can exist at the tops of the surfaces due to the trapped air in the cavity regions, which increases with the relative size of the cavity regions [10]. Further, the liquid-surface contact angle increases significantly. These two effects exercise influence on the overall dynamics of the droplet spread and subsequent collapse. In general, increasing superhydrophobicity can lead to increased rebound velocity [11]. A recent paper by Butt et al. provides an excellent overview of characteristics of superhydrophobic surfaces, droplet rolling, impalement, and collisions [12]. It is important to note that the size of the structuring considered here is much smaller than the thickness of the thin film for the expanding droplet, and consequently thin film rupture and accompanying droplet splitting does not occur.

A recent paper by Pearson et al. explored droplet impingement on anisotropic superhydrophobic surfaces that exhibit alternating rib and cavity features [11], with cavity widths of nominally 32 μm. Such features result in the contact angle and apparent slip at the surface varying tangentially, with the apparent slip being a maximum along the direction of the ribs/cavities (longitudinal direction) and the advancing and receding contact angles being a maximum in the transverse direction (perpendicular to the ribs/cavities). Two liquid types were explored in the earlier study, water and a 50%/50% by weight mixture of water and glycerol. An interesting observation from this work is that at impact Weber numbers, $We = \rho V^2 D/\sigma$, greater than 70 the maximum spread in the longitudinal direction exceeds the spread in the transverse direction and the difference between these two quantities increases with increasing We. ρ is the liquid density, V is the droplet velocity at impact, D is the droplet diameter at impact, and σ is the liquid surface tension. This previous work characterized for the first time the maximal spread diameter in the two primary spreading directions (along and transverse to the ribs) for both fluid types explored. A related and important result is that under a certain range of conditions, the collapsing and rebounding droplet was observed to exhibit a unique and previously unreported two-pronged jet emission. This is illustrated in Fig. 1 where the two-pronged emission is shown in the left panel of Fig. 1, whereas in the right panel the jet emission when the two-pronged emission does not prevail is shown for comparison. This two-prong behavior is only manifest during the recoiling phase of the droplets' motion. Note that the camera viewing angle and the lighting were slightly different for the two images of Fig. 1, even though the surface characteristics were exactly the same.

A second recent paper also explored droplet impingement on superhydrophobic surfaces with alternating ribs and cavities [13]. However, the spacing between ribs in this study was 173 μm, 5.4 times greater than the width used by Pearson et al. and thus the wettability of the surfaces is much greater. It is unlikely that during droplet collision the Cassie state was maintained in their study. They also observed anisotropy in the collision process, with two prongs appearing. However, their results reveal the two prongs forming during the spreading phase, as opposed to the recoiling phase. This is likely caused by liquid penetrating the cavities during the collision process and being expelled outward along the cavities and resulting in greater mass moving parallel to the cavities than transverse to them.

The previous paper by Pearson et al. observed for the first time the existence of two-pronged jet emission during the recoiling

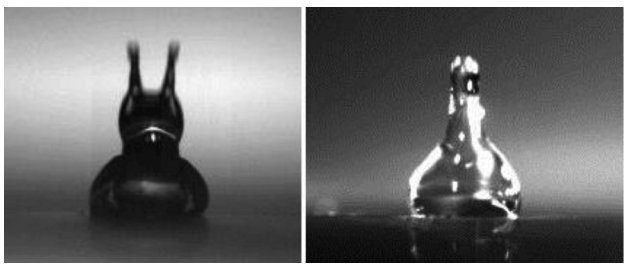

Fig. 1 Example images of droplet impingement on anisotropic superhydrophobic surfaces under conditions where the two-pronged jet emission occurs (left) and where it does not (right)

[1]Corresponding author.

Contributed by the Fluids Engineering Division of ASME for publication in the JOURNAL OF FLUIDS ENGINEERING. Manuscript received June 10, 2015; final manuscript received December 30, 2015; published online April 22, 2016. Assoc. Editor: John Abraham.

process, but only for a single Ohnesorge number, $\mathrm{Oh} = \mu/\sqrt{\rho\sigma D} \approx 0.01$. The focus of this paper is to completely characterize the parameter space over which such two-pronged jet emission may be expected to occur, which gives insight into the fundamental mechanisms affecting the spread and recoil of droplets impinging on rib/cavity structured superhydrophobic surfaces. Specifically, we report experimental results that quantify the range of Ohnesorge numbers and Capillary numbers, $\mathrm{Ca} = V\mu/\sigma = \mathrm{We}^{1/2}\mathrm{Oh}$, over which such two-pronged jet emission occurs, where μ is the liquid viscosity. Experiments were conducted for 11 different liquids spanning the range $0.0017 \leq \mathrm{Oh} \leq 3.0$. This corresponds to liquids varying in viscosity over more than three orders of magnitude and the results of this paper completely define the range of parameters over which two-prong jets are expected to form on anisotropic superhydrophobic surfaces.

2 Methodology

Droplet impact experiments were performed on a flat horizontal surface. The droplets were released from a hypodermic needle at varying heights above the surface of interest to vary the impact speed. The droplet diameter was varied within the nominal range of 2 mm up to 6 mm using different needle sizes and the impingement process was recorded with a 1024×1024 Photron FASTCAM APX RS high-speed camera at 6000 frames per second. The resulting images were processed to obtain the droplet impact diameter, D, and impact velocity, V. These values, along with the fluid properties (ρ, μ, and σ), were used to calculate the dimensionless parameters of interest, namely, Oh and Ca.

The surface employed in the experiments consisted of microribs and cavities which were then coated with Teflon [10]. A scanning electron microscope (SEM) image of one of the structured and Teflon-coated surfaces used is provided in Fig. 2. Noted on the figure are the parameters w_c, the width of a cavity, and w, the combined rib and cavity module width. The cavity fraction for all experiments reported in this study is $F_c = w_c/w = 0.93$. The combined rib/cavity module width was $w = 40\,\mu$m and the cavities were 15 μm deep.

In order to fully explore the two-pronged jet phenomenon, fluid properties were varied using mixtures of water and glycerol. Eleven different concentrations of glycerol were used in total, as shown in Table 1, where fluid properties are specified according to the percentage of glycerol (by mass). The mixture viscosity, surface tension, and density were determined from the literature [14–16]. As is illustrated in Table 1, viscosity varies by more than three orders of magnitude, while density and surface tension each vary by nominally 13%.

The impingement event was recorded from the two normal directions: the longitudinal direction (liquid spreading/collapsing parallel to the ribs) and the transverse direction (spreading/collapsing perpendicular to the ribs). The liquid–solid advancing and receding contact angles were measured using a goniometer and the standard liquid addition approach to quantify advancing and receding angles. This was done for the case of pure water and the 50% glycerol mixture and these values are shown in Table 2, with an uncertainty of nominally 1 deg. As illustrated by the data of Table 2 the contact angles for these two are nearly the same. The contact angles of the remaining concentrations of glycerol were all similar to those shown in Table 2, with the contact angles decreasing slightly with increasing glycerol concentration.

The high-speed video images were used to determine under what conditions the two-pronged jet emission occurs. The images were also analyzed to determine the maximum spread diameter of the droplets during the impingement process. Detailed information on the experimental uncertainty can be found by Pearson et al. [11]. The uncertainties in the maximum spreading diameter, the impact Capillary number, and the Ohnesorge number were 7.7%, 5.3%, and 5.1%, respectively.

Table 1 Density, viscosity, and surface tension for all fluids employed in the experiments determined from the literature [14–16]

% glycerol	Density, ρ (kg/m^3)	Viscosity, μ (MPa·s)	Surface tension, σ (mN/m)
0 (pure water)	998	0.959	72.7
12.5	1014	1.341	72.07
25	1030	2.001	71.28
37.5	1046	3.254	70.32
45	1056	4.601	69.67
50	1062	5.9	69.2
55	1068	7.947	68.71
58.75	1073	10.06	68.32
67.5	1084	18.97	67.36
75	1094	36.84	66.48
100	1126	1500	63.1

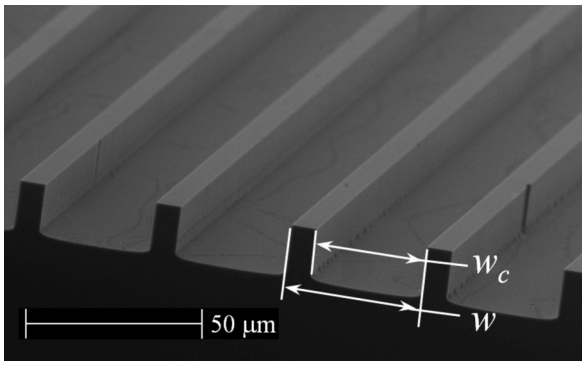

Fig. 2 SEM image of a superhydrophobic surface comprised of alternating rib and cavity structures. The cavity width, w_c, and the combined rib and cavity width, w, are shown.

3 Results

The qualitative two-pronged emission is illustrated in Fig. 3, where five sequences of photographic images during the droplet impact, spread, collapse, and jet emission process are shown. All five sequences were taken at $\mathrm{Oh} \approx 0.013$, which is typical for the 50% glycerol mixture. Shown are images for the Ca regime just prior to where the two-pronged phenomenon was observed (Fig. 3(*a*)), images of the two-pronged jets from the transverse view (Fig. 3(*b*)), images of the two-pronged jets from the longitudinal view (Fig. 3(*c*)), images showing a top view (ribs and cavities oriented top to bottom on the images) (Fig. 3(*d*)), and images for the Ca regime after two-pronged jets are no longer observed and where fingering and prompt splash are the dominant features (Fig. 3(*e*)). Figures 3(*a*) and 3(*e*) show the transverse view. The images show, from top to bottom, a droplet at impact (time = 0 ms), as the jet is first visible (7.5 ms), and two images showing jet progression (8.2 and 10 ms).

Table 2 Advancing and receding contact angles in the longitudinal (*L*) and transverse (*T*) directions for pure water and the 50% glycerol mixture

	Contact angle, θ (deg)			
	Water		50% Glycerol mixture	
Rib orientation	Advancing	Receding	Advancing	Receding
T	167.3	156.7	165.1	151.1
L	160.7	155.2	161.2	154.5

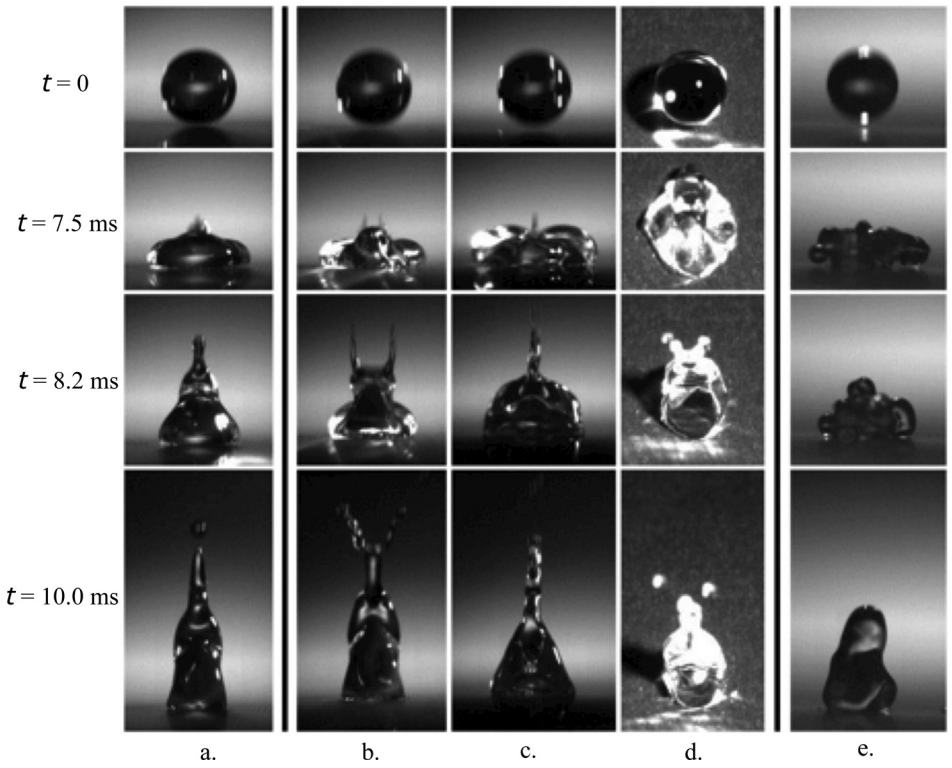

Fig. 3 Shown are images for (*a*) the Ca regime just before two-pronged jets, two-pronged jets from (*b*) the transverse view, (*c*) the longitudinal view, (*d*) the top view, and (*e*) the regime just after two-pronged jets. For all image sets, Oh = 0.013. Images show, from top to bottom, a droplet at impact (time = 0 ms), as the jet is first visible (7.5 ms), and two frames showing jet progression (8.2 and 10 ms). Parts (*a*) and (*e*) show the transverse view.

For the case where Ca is below the range where two prongs are observed (Fig. 3(*a*)), the jet is seen rising as a single coherent jet throughout the process, as is typically observed for droplet impact on hydrophobic surfaces. As seen in Figs. 3(*b*)–3(*d*), the two-pronged jets are primarily evident in the transverse direction. When viewed in the longitudinal direction (Fig. 3(*c*)), the two prongs lie in the same plane and appear as a single jet. The final image set, Fig. 3(*e*), shows the instabilities that are characteristic of droplets impacting a surface at high Ca, beyond the range where two-pronged jets are observed. These instabilities, evident in the fingering and splashing that occur, are likely the reason that two-pronged jets are no longer observed.

A physical explanation for the formation of the two-pronged jets is evident in Fig. 3(*d*), the top view of the spreading and collapsing process. It can be seen that the droplet spreads and retracts at different rates in the two primary directions, the longitudinal and transverse directions. This unequal retraction, caused by the anisotropy of the surface and the resulting unequal shear stresses and contact angles, results in the fluid retracting completely in the longitudinal direction first. A noncircular jet is then ejected with the fluid pulling away from the center causing a temporary separation into two coherent prongs. As the two prongs rise, the inward motion and surface tension pull causes the prongs to eventually coalesce into a single jet, frequently after emitting two separate upward traveling droplets.

All data acquired for the different droplet diameters and fluids were analyzed (over 800 independent experiments) and the data is best correlated in terms of the Capillary and Ohnesorge numbers. Figure 4 presents data up to Oh of 0.02, although data were acquired all the way to Oh $\approx$ 3.0. Red markers correspond to the events when two prongs were observed during rebound and the blue markers correspond to the events when two prongs were not observed. Indicated on the plot are upper and lower bound curve fit lines (and there corresponding equations) that define the region where two-pronged jets are observed, where they are not observed, and where they are interrupted by fingering and/or splashing. It can be seen that the Ca range where two-pronged jets are observed is very narrow at low Oh and increases to a fairly

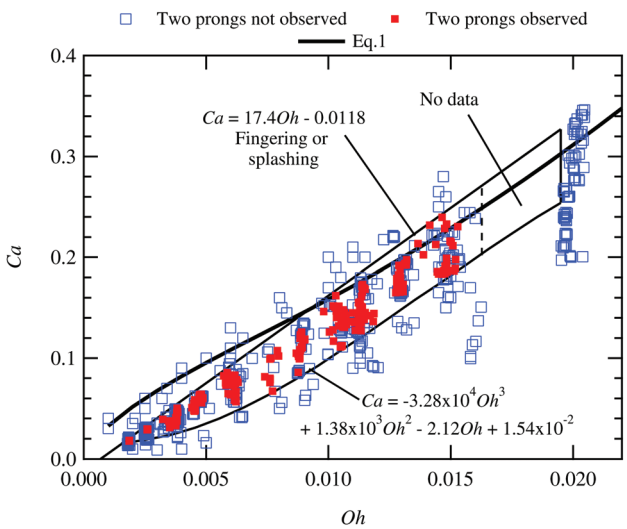

Fig. 4 Plot of Capillary number, Ca, against Ohnesorge number, Oh. Impingement events that resulted in a two-pronged jet are shown in red and the scenarios that did not result in two-prong rebound are shown in blue. Equations for the upper and lower lines bounding the two-pronged jet regime are noted on the plot, with the fingering and/or splashing regime existing above the upper bounding line. Also shown is Eq. (1), a prior correlation from Ref. [17] to predict the onset of splashing for impact onto a dry surface.

constant range by Oh ≈ 0.007. There is a portion on the plot where there was no data acquired. This represents the region where Oh would correspond to a fluid with properties between those of the 55% and 58.75% glycerol mixtures. No two-pronged jets were observed above Oh = 0.0154 (the 58.75%, 67.5%, 75%, and 100% glycerol mixtures), although a gap in data exists between Oh = 0.0154 (55% mixture) and Oh = 0.0195 (58.75% mixture).

Recent works have defined the splash threshold for drop impact onto a dry substrate [17–19]. At impact Reynolds numbers in the range considered in this study, Palacios et al. [17] suggested the following correlation for the critical Weber number at which droplets are formed:

$$\mathrm{We}_{\mathrm{splash}} = 5.8\sqrt{\mathrm{Re}} + 4.01x10^{7}\,\mathrm{Re}^{-1.97} \quad (1)$$

Equation (1) can be recast in terms of Ca and Oh and the resulting equation is shown in Fig. 1, where values above the line correspond to where a splash is predicted. Equation (1) differs modestly from the observed transition line between where two-prong jets were observed and where they were never observed. At low values of Oh (<0.008) this difference is likely due to fingering that occurs (prior to splashing), which distorts the retraction process and causes a more chaotic recoil and jet formation. The literature does not give predictions for the onset of fingering, which happens slightly below the onset of splashing. It should be noted that the splashing threshold has been shown previously to depend on the surrounding ambient pressure [20].

As illustrated in Fig. 4, the two-pronged jets are not observed for every experimental trial in the regime where they occur, likely due to initial asymmetries or oscillations in the droplet prior to impact and that are formed during the droplet release and flight. The probability of the two-pronged jets is characterized in Fig. 5 as a function of Oh. Probability within each range of Oh shown in Fig. 5 was determined using data for all Ca values that fell within the bounds where two-pronged jets were observed in Fig. 4. The probability of occurrence is also a function of Ca, as suggested by the data of Fig. 4. At a given value of Oh, the greatest likelihood of occurrence occurs at a value of Ca that is approximately midway between the upper and lower bounding lines shown in Fig. 4. The previous work describing two-pronged jets [11] provides the probability of two-pronged jets for the 50% glycerol mixture (Oh ≈ 0.011–0.012) as a function of We (or Ca). At Oh ≈ 0.011, the probability of occurrence increased from approximately 0.2 at the lower bounding limit to approximately 0.65 at a value of Ca midway between the two bounding limits. It then decreased to nominally 0.15 at the upper bounding line. A similar distribution in probability with varying Ca prevails for each fluid type (varying Oh) explored here, although additional data are necessary to accurately define the probability distribution as a function of both Oh and Ca. Over the full parameter range where two-pronged jets were observed (seen in Fig. 4), the overall probability of occurrence was 50%.

The reason that the two-pronged jets no longer exist above Oh ≈ 0.00195 is likely due to the reduced spread of the droplet concomitant with increasing viscosity. The influence of the superhydrophobic surface on the droplet motion increases as the droplet spread increases, since at larger spread diameters the droplet thickness decreases significantly. It has been well established that the influence of superhydrophobicity on apparent slip at the surface is more manifest as the thickness of the liquid layer decreases [10]. Thus, at large Oh, where the spread is smaller, the difference in the influence of the surface on the droplet spread and retraction in the two primary spread directions is small. However, when the droplet spread is greater, the anisotropy of the surface and the thinness of the spreading droplet together result in varying slippage along the two primary spreading directions, which gives rise to the two-pronged jets. Clavijo et al. have presented an analytical model of drop impact on anisotropic surfaces and their model results reveal droplet spreading that is consistent with this explanation [21]. It should also be noted that we have also conducted a wide array of experiments on surfaces with poststructured features of similar cavity fraction as the rib-cavity surfaces. Two pronged jet emission was not observed for these surfaces at any impact condition, supporting the hypothesis that the formation is caused by anisotropy in the apparent fluid slip at the surface.

Figure 6 shows the relative maximum diameter spread in the transverse spread direction, D_m/D, as a function of Oh for three values of We (100, 150, and 200), where D is the droplet diameter just prior to impact and D_m is the droplet diameter at the point of maximum spread. Because the two-pronged jets are visible only in the transverse direction, data for the longitudinal direction was not collected. The relationship between the two directions has been described previously [10]. Each data point represents the maximum relative spread calculated using a least-squares fit to a small range of data taken at the given value of Oh. Also shown in Fig. 6 is a dashed polygon shape that defines for what scenarios the two-pronged behavior prevails. In addition, least-squares power law fits to the We = 100 and 200 data sets are shown on the figure. As can be seen, the droplet spread decreases as Oh increases for all values of We until they essentially converge at Oh ≈ 3, which corresponds to 100% glycerol. D_m/D ranges from nominally 3 (We = 100) to 3.3 (We = 200) at the bound between two-pronged jet occurrence and the existence of fingering or

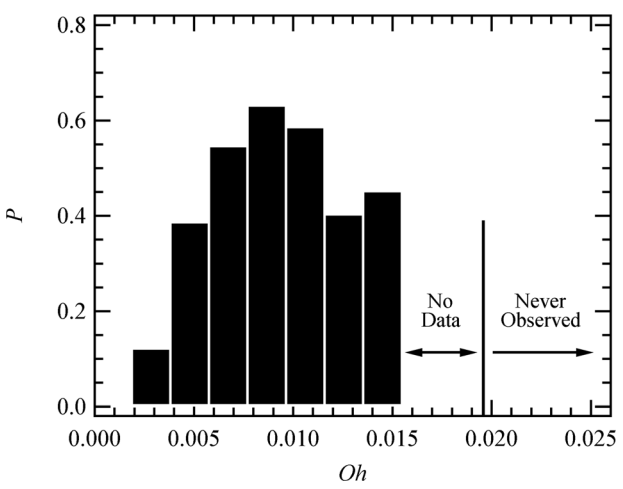

Fig. 5 Probability, *P*, of observance of two-pronged jets as a function of Oh. Probability is taken within the region of Ca where two-pronged jets are observed.

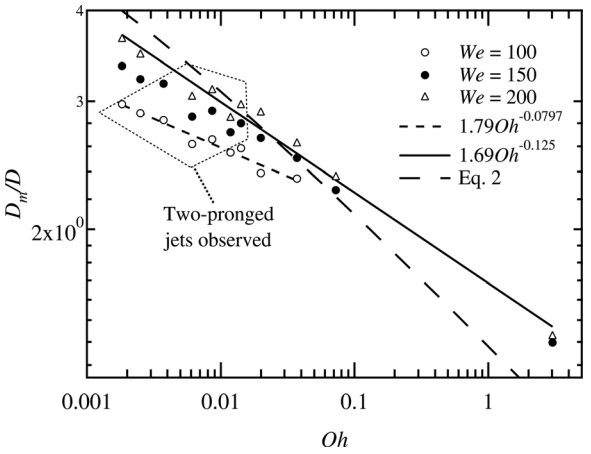

Fig. 6 Plot of maximum relative diameter in the transverse spread direction, $D_m/2$, as a function of Oh. Maximum diameter data was taken at three Weber numbers, as shown. Also shown are least-squares power law fits to the data for We = 100 and 200 and a line corresponding to Eq. (2), where We = 200.

splashing. At the lower bound D_m/D ranges between 2.6 and 3. Figure 6 represents D_m/D data over the largest range of Oh that have been reported in the literature to date, and the overall variation in D_m/D as a function of Oh is a secondary but important result from this work.

Also shown in Fig. 6 is a line corresponding to Eq. (2), with We held constant at a value of 200

$$\frac{D_m}{D_i} = 0.87\mathrm{We}^{1/10}\mathrm{Oh}^{1/5} - \beta\mathrm{We}^{-3/10}\mathrm{Oh}^{-2/5} \tag{2}$$

Equation (2) follows Eq. (13) in Ref. [12], where these authors propose the value of $\beta = 0.48$ to best match available experimental data. Note that prior experimental data has generally included only relatively small values of Oh, with water being the most common liquid considered. Figure 6 reveals good agreement between our present data and Eq. (2) for $\mathrm{We} = 200$ and at values of Oh typical for previous studies. As Oh gets very large (≈ 3), much greater deviation between our data and Eq. (2) exists and this feature deserves future attention.

4 Conclusions

Droplet impingement experiments have quantified the parameter ranges where the two-pronged jet phenomenon is likely to occur on anisotropic superhydrophobic surfaces comprised of ribs and cavities. It was determined that Oh and Ca are the primary influencing parameters. Two-pronged jets were never observed above $\mathrm{Oh} = 0.0154$. For increasing Oh, the range of Ca where two-pronged emission is observed increases. The two-pronged jets are most likely caused by unequal droplet spreading and retraction velocity that is a result of the anisotropic surfaces that were employed in the study. They are not observed for high Oh due to the smaller spread diameter and concomitant thicker droplets, characteristic of high viscosity fluids. Impingement experiments conducted on superhydrophobic surfaces that exhibit isotropic slip have also been conducted, where two-prong jet formation was not observed, supporting this hypothesis.

References

[1] Yarin, A. L., 2006, "Drop Impact Dynamics: Splashing, Spreading, Receding, Bouncing…," Annu. Rev. Fluid Mech., **38**(1), pp. 159–192.

[2] Shirtcliffe, N. J., McHale, F., Atherton, S., and Newton, M. I., 2010, "An Introduction to Superhydrophobicity," Adv. Colloid Interface Sci., **161**(1–2), pp. 124–138.

[3] Li, X. M., Reinhoudt, D., and Crego-Calama, M., 2007, "What Do We Need for a Superhydrophobic Surface? A Review on the Recent Progress in the Preparation of Superhydrophobic Surfaces," Chem. Soc. Rev., **36**(8), pp. 1350–1368.

[4] Clanet, C., Beguin, C., Richard, D., and Quéré, D., 2004, "Maximal Deformation of an Impacting Drop," J. Fluid Mech., **517**, pp. 199–208.

[5] Ukiwe, C., and Kwok, D. Y., 2005, "On the Maximum Spreading Diameter of Impacting Droplets on Well-Prepared Solid Surfaces," Langmuir, **21**(2), pp. 666–673.

[6] German, G., and Bertola, V., 2009, "Review of Drop Impact Models and Validation With High-Viscosity Newtonian Fluids," Atomization Sprays, **19**(8), pp. 787–807.

[7] Marengo, M., Antonini, C., Roisman, I. V., and Tropea, C., 2011, "Drop Collisions With Simple and Complex Surfaces," Curr. Opin. Colloid Interface Sci., **16**(4), pp. 292–302.

[8] Brunet, P., Lapierre, F., Thomy, V., Coffinier, R., and Boukherroub, R., 2008, "Extreme Resistance of Superhydrophobic Surfaces to Impalement: Reversible Electrowetting Related to the Impacting/Bouncing Drop Test," Langmuir, **24**(19), pp. 11203–11208.

[9] Lembach, A. N., Tan, H. B., Roisman, I. V., Gambaryan-Roisman, T., Zhang, Y., Tropea, C., and Yarin, A. L., 2010, "Drop Impact, Spreading, Splashing, and Penetration Into Electrospun Nanofiber Mats," Langmuir, **26**(12), pp. 9516–9523.

[10] Rothstein, J. P., 2010, "Slip on Superhydrophobic Surfaces," Annu. Rev. Fluid Mech., **42**(1), pp. 89–109.

[11] Pearson, J. T., Maynes, D., and Webb, B. W., 2012, "Droplet Impact Dynamics for Two Liquids Impinging on Anisotropic Superhydrophobic Surfaces," Exp. Fluids, **53**(3), pp. 603–618.

[12] Butt, H.-J., Roisman, I. V., Brinkmann, M., Papadopoulos, P., Vollmer, D., and Semprebon, C., 2014, "Characterization of Super Liquid Repellent Surfaces," Curr. Opin. Colloid Interface Sci., **19**(4), pp. 343–354.

[13] Kannan, R., and Sivakumar, D., 2008, "Drop Impact Process on a Hydrophobic Grooved Surface," Colloids Surf., A, **317**, pp. 694–704.

[14] Cheng, N., 2008, "Formula for the Viscosity of a Glycerol-Water Mixture," Ind. Eng. Chem. Res., **47**(9), pp. 3285–3288.

[15] Incropera, F. P., Dewitt, D. P., Bergman, T. L., and Lavine, A. S., 2007, *Fundamentals of Heat and Mass Transfer*, 6th ed., Wiley, Hoboken, NJ.

[16] Deng, Q., Anilkumar, A. V., and Wang, T. G., 2007, "The Role of Viscosity and Surface Tension in Bubble Entrapment During Drop Impact Onto a Deep Liquid Pool," J. Fluid Mech., **578**, pp. 119–138.

[17] Palacios, J., Hernandez, J., Gomez, P., Zanzi, C., and Lopez, J., 2013, "Experimental Study of Splashing Patterns and the Splashing/Deposition Threshold in Drop Impacts Onto Dry Smooth Solid Surfaces," Exp. Therm. Fluid Sci., **44**, pp. 571–582.

[18] Roisman, I. V., Lembach, A., and Tropea, C., 2015, "Drop Splashing Induced by Target Roughness and Porosity: The Size Plays No Role," Adv. Colloid Interface Sci., **222**, pp. 615–621.

[19] Wal, R. L. V., Berger, G. M., and Mozes, S. D., 2006, "The Splash/Non-Splash Boundary Upon a Dry Surface and Thin Fluid Film," Exp. Fluids, **40**(1), pp. 53–59.

[20] Xu, L., Zhang, W. W., and Nagel, S. R., 2005, "Drop Splashing on a Dry Smooth Surface," Phys. Rev. Lett., **94**(18), p. 184505.

[21] Clavijo, C. E., Crockett, J., and Maynes, D., 2015, "Effects of Isotropic and Anisotropic Slip on Droplet Impingement on a Superhydrophobic Surface," Phys. Fluids, **27**, p. 122104.